IEEE Access
Multidisciplinary ⋮ Rapid Review ⋮ Open Access Journal

Received January 14, 2021, accepted January 23, 2021, date of publication January 26, 2021, date of current version February 4, 2021.

Digital Object Identifier 10.1109/ACCESS.2021.3054825

A New Technique on Vibration Optimization of Industrial Inclinometer for MEMS Accelerometer Without Sensor Fusion

MINH LONG HOANG, (Member, IEEE), AND ANTONIO PIETROSANTO, (Senior Member, IEEE)
Department of Industrial Engineering, University of Salerno, 84084 Fisciano, Italy

Corresponding author: Minh Long Hoang (mhoang@unisa.it)

This work was supported by the University of Salerno, Italy, through the European Union on the Nationally Operative Program (PON) Doctorates Project for Industrial Research and Innovation, collaboration between the University of Salerno and Sensor System Company.

ABSTRACT Accelerometer of the Microelectromechanical systems (MEMS) based inertial measurement units (IMUs) is key to inclination measurement in the industry 4.0. However, external vibration negatively impacts the precision of orientation angles during operation. Many inclinometer companies have demanded to develop a solution for vibration impact on accelerometer without other sensors' support because of economic problems. This article presents a new algorithm Orientation Axes Crossover Processing (OACP) on vibration optimization for MEMS accelerometer without sensor fusion. The proposed filter works on a principle based on the characteristics of vibration impact on whether the X-axis or Y-axis to optimally minimize the noise. A high accurate setup is built-up based on the Pan-Tilt Unit and a TUMAC vibrator for the verification of new filters, implemented into LSM9DS1 (3D accelerometer, 3D gyroscope). The new filter is able to work independently, and also fuse with the Low-pass filter or Kalman filter to enhance the dynamic response, only 0.163 seconds as maximum delay during vibration. The experimental results show that the proposed algorithm always accomplishes smaller variations than Low-pass filter, about 0.2 degrees in standard deviation. The compromise between vibration immunity and dynamic response is analyzed in detail to demonstrate the optimal performances of the concerned filters. The project was carried out at the 'Sensor System' in Italy which is an industrial company in the inclinometer field.

INDEX TERMS MEMS, IMUs, accelerometer, gyroscope, low-pass filter, Kalman filter, sensor fusion.

I. INTRODUCTION

Microelectromechanical system (MEMS) accelerometer is a highly advanced technology for measuring linear acceleration, vibration, especially orientation angles [1]–[7] . This sensor type has become an indispensable factor in the industry 4.0 as an inclinometer for Rotary Drilling Rig, robotic and other vehicles [8]–[11].

In reality, the vehicle and machine operation, especially in heavy industry, produce vibration noise, which affects the acceleration measurement data of the Inertial Measurement Unit (IMU) sensor [12]–[14]. The vibration [15] causes considerable variations in the inclinational data that mislead the whole system's performance. The accelerometer calibration [9], [11], [16]–[18] corrects the acceleration to its proper value under normal condition, but these calibration methods cannot solve the vibration issue.

Kalman filter [19], [20], is the popular method that removes the noise of MEMS by the sensor fusion between accelerometer, gyroscope, and magnetometer [21]–[23]. The magnetometer is usually not required for the inclinometer because the magnetic data is used for heading estimation. Meanwhile, acceleration and angular rates are necessary for the tilt calculation [24]. Practically, many inclinometer companies have been demanding an effective filter for only accelerometer without the support from other sensors because of economic concern when numerous inclinometers are in production. The Low-pass (LP) filter is a solution for the vibration immunity [25], [26], which can work on the accelerometer independently. The LP filter removes high-frequency noise based on the adjustable coefficient. The main problem of this filter is the difficulty of balance between the

The associate editor coordinating the review of this manuscript and approving it for publication was Shih-Wei Lin.

dynamic response and vibration elimination. The LP coefficient may be selected to linearize the vibration noise absolutely, but its dynamic response is decreased considerably.

In industry, the inclination sensor measures two parameters: rotation around the front to-back X-axis, called roll, rotation around the side-to-side Y-axis, called pitch [28]. This article presents a filter with a new algorithm Orientation Axes Crossover Processing (OACP) which works on the vibration impact's characteristics, whether X-axis or Y-axis. If vibration mainly occurs on X-axis, the roll will suffer considerable variation while pitch gets small change. Therefore, the OACP filter sets up a suitable threshold based on two consecutive samples of Y-axis acceleration (*Yacc*) to whether the X-axis acceleration (*Xacc*) is used for roll calculation or not and vice versa for pitch evaluation. The ''Axes Crossover'' principle is processed by using a threshold of acceleration variation on the X-axis ($\Delta Xacc$) to optimize the Y angle and threshold of acceleration variation on the Y-axis ($\Delta Yacc$) to optimize X angle. This threshold is updated practically, based on vibration characteristics.

The OACP filter is able to fuse with other filters such as the LP filter and the Kalman filter:

- The filter fusion is the combination of LP filter and OACP filters
- Kalman_acc filter is named for the implementation of the OACP technique into the Kalman filter. This method requires only the accelerometer to enhance its dynamic response without gyroscope support.

On the other hand, the vibrations impact are taken into account for both static and dynamic cases. The static case is analyzed when the sensor on the Earth frame; no dynamic motion is applied. The dynamic test shows how each kind of filter handles the fluctuation of the external noise during the motion and how fast they achieve a stable result when the dynamic motion ends.

The paper is organized as follows: Initially, it is about the introduction to the inclination formula, then a brief description of the traditional filters: LP filter and Kalman filter (sensor fusion between accelerometer and gyroscope). The next part focuses on the OACP filter with the update algorithm then the combination between multiple filters. Finally, experimental results and signal characterization with the conclusion will be shown at the end of the paper.

A. INCLINATION MEASUREMENT

To measure roll and pitch, various formulas have been applied [29], [30]. In this work, 2 fundamental formulas are used for oriental inclination. Both of 2 angles process in the range of $[-90° - 90°]$.

The *Xacc* is proportional to the sine of the angle of inclination (Roll). The *Yacc* is corresponding to the cosine of the angle of inclination (Pitch). Roll and pitch under vibration are characterized, based on the acceleration of the X-axis and Y-axis respectively as shown relationship in Eq. (1) and Eq. (2). Fig. 1 illustrates the relative curve between

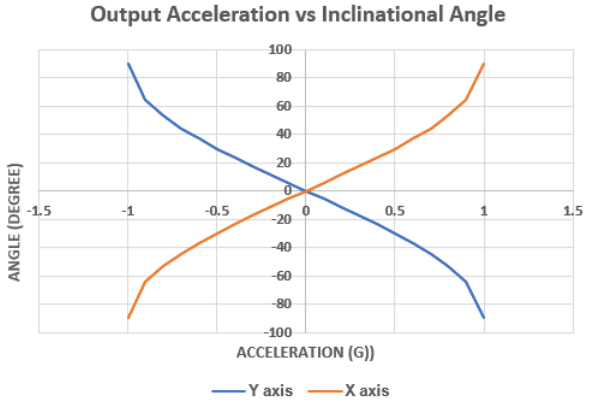

FIGURE 1. Acceleration vs angle.

FIGURE 2. Chart of LP filter.

acceleration and corresponding angle on X-axis and Y-axis.

$$Roll = arcsin(Xacc) \tag{1}$$

$$Pitch = arccosin(Yacc) - 90 \tag{2}$$

II. TRADITIONAL FILTERS

In this part, the LP filter and Kalman filter, 2 most popular filters are introduced for noise reduction. Their functions are described clearly by the mathematical models.

A. LP FILTER

This filter is a useful tool to remove high-frequency noise by allowing only low-frequency signals to pass through, as demonstrated in Fig.2. In this system, a simple but effective LP filter is designed based on the below algorithm.

$$y_t = (\alpha) * (y_{t-1}) + (1 - \alpha) * (y_t) \tag{3}$$

where: α is the filter coefficient; y_t and y_{t-1} are output acceleration at the current sample and the previous sample respectively

The filter coefficient can be evaluated based on the time period (τ) of the desired cut-off frequency (*fcut*) and loop time (*dt*) of the accelerometer output data rate

$$\tau = \frac{1}{f_{cut}} \tag{4}$$

$$\alpha = \frac{\tau}{\tau + dt} \tag{5}$$

where the acquisition value from accelerometer are *Xacc* and *Yacc* as the inputs of the LP filter and X and Y defined as outputs acceleration.

B. KALMAN FILTER

The Kalman filter fuses the input data by combing uncertain measurement and uncertain control system models [31].

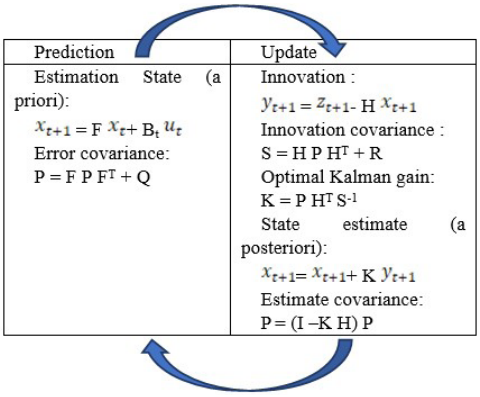

FIGURE 3. Kalman operating principle.

Usually, the procedure is carried out by a series of measures over time from the accelerometer and gyroscope to minimize the noise of the inclination signal. The prediction and update are two main processes to work in a Kalman filter like described in Fig.3. Thanks to the OACP filter, the Kalman algorithm can be applied to an accelerometer independently with potent function. Here, a traditional but active Kalman filter is described briefly based on the current and previous states.

$$x_{t+1} = F.x_t + B_t.\mu_t + \omega_t \tag{6}$$

$$z_{t+1} = H.x_{t+1} + v_{t+1} \tag{7}$$

where x_t, x_{t+1} represent the system state vectors at time t and $t+1$ respectively; μ_t is the input vector at time t, z_{t+1} is the observation (or measurement) at time $t+1$.

F is the state transition model which relates the current states to the next states

- B_t is the control input model which is applied to the control vector μ_t
- H is the observation model which maps the true state space into the observed space
- ω_t is the state noise, which is attained by covariance matrix $Q[k]$ where $\omega \simeq N(0, Q)$

$$Q[k] = \begin{pmatrix} Q_{acc} & -\Delta \\ 0 & Q_{bias} \end{pmatrix} \tag{8}$$

This matrix is composed of the estimated state from the accelerometer variance Q_{acc} and the variance of bias Q_{bias} multiplied by the time interval ΔT.

- Like w_t, with R is the variance of the measurements, μ_t is the noise measurement $\mu_t \simeq N(0, R)$.
- For the traditional method, the orientation angles are calculated from the LP filter data, then fuse with the angular rate (ω_x, ω_y) as in Fig.4
- For the case of combination between Kalman and OACP filter, the OACP data, is directly fused with the inclination data from the LP filter, as Fig.5, This fusion technique generates Kalman outputs (Roll_Kalman_acc and Pitch_Kalman_acc), which require only accelerations as inputs.

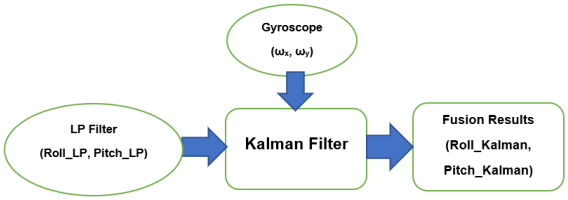

FIGURE 4. Chart of Kalman filter (sensor fusion).

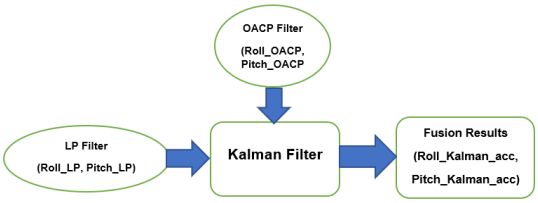

FIGURE 5. Chart of Kalman_acc filter.

III. OACP FILTER

A. OPERATING PRINCIPLE

Practically, the vibration can strongly influence on X-axis or Y-axis for a specified time. The OACP filter works on the difference between absolute values of 2 consecutive acceleration samples of each axis ΔX, ΔY.

$$\Delta X = abs(|X_n| - |X_{n-1}|) \tag{9}$$

$$\Delta Y = abs(|Y_n| - |Y_{n-1}|) \tag{10}$$

where n is the index of the current sample; X and Y are the filtered acceleration from the LP filter. Not only during vibration but also the dynamic inclination of the X-axis (roll), ΔY has a small variation in mg while ΔX has significant value. Similarly, when vibration occurs on Y-axis or while pitch rotates, ΔX has a slight variation, in contrast to the high value of ΔY.

According to orientation formula in Eq. (1) and Eq. (2), roll measurement requires good immunity to vibration on the X-axis for the *Xacc*. Pitch measurement needs high vibration immunity for *Yacc*. A threshold is set as the boundary for vibration and the axis position of inclination. The OACP filter works on the threshold of the axis, which has the lowest variation value in each vibration case. This function is straightforward and highly effective for vibration characteristics. ΔX threshold, ΔY threshold are selected with narrow but suitable value.

As illustrated in Fig.6 :

- If the vibration on X-axis and motion occur on the roll, ΔY get the least variation

$\Rightarrow$ OACP filter has the primary role in optimizing the vibration impact on roll (a strong variety on X_{acc}) by using ΔY threshold condition.

- If the vibration on X-axis and motion occur on the roll, ΔX get the lowest variation.

$\Rightarrow$ OACP filter has the main role in optimizing the vibration impact on the pitch (a strong change on Y_{acc}), by using ΔX threshold condition.

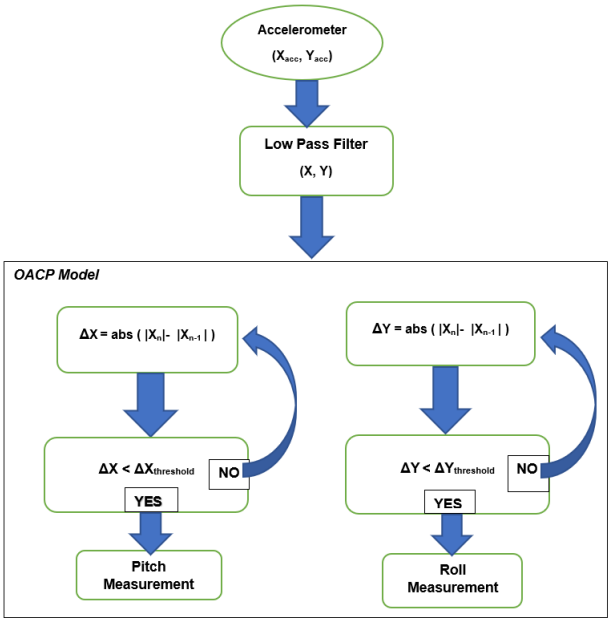

FIGURE 6. OACP filter diagram.

- The OACP principle :

Once the energetic vibration occurs on the sensor, both X-axis and Y-axis suffer the variation. However, the amplitude of variation is the difference between ΔX and ΔY, depends on whether vibration mainly impacts right-left (X-axis) or forward-backward (Y-axis).

Vibration mainly befalls on Y-axis:

$\Rightarrow$ Pitch needs to be filtered adequately.
$\Rightarrow$ ΔX varies less than ΔY and has a better stability.
$\Rightarrow$ The threshold on X-axis is selected because now, ΔY has a significant variation $\Rightarrow$ ΔY threshold must be big and more difficult to collect.
$\Rightarrow$ Since vibrations cause ΔX to vary under ΔX threshold, no noise calculation can be accumulated in pitch.

In that way, the same principle is carried out when vibration on X-axis. ΔX threshold is collected to prevent noise from the roll

If $\Delta X < \Delta X$ threshold $\Rightarrow$ pitch calculation
If $\Delta Y < \Delta Y$threshold $\Rightarrow$ roll calculation

B. THRESHOLD UPDATE

To be practical, the threshold must be updated which depends on the vibration characteristic. After numerous tests, the starting threshold is supposed to be $1mg$. This value is suitable since the crossing threshold is chosen, based on the axis variation when the vibration does not occur directly like a detailed analysis in the previous part. Here, Δ_{acc} is the absolute variation value between 2 acceleration samples. Δth is the threshold value of Δ_{acc}.

During mechanical operation, vibrations happen fast with high frequency. Two counters set up:

- Counter_up: When stronger vibration causes a more significant value of Δ_{acc}, so Δth increases.

TABLE 1. Threshold update model.

Vibration Changes	Update Procedures
Stronger	If ($\Delta\_acc > \Delta th$): {counter_up +=1}; For 1 second, if (counter_up $\geq$ ODR/3) { Δth += 0.2}
Weaker	If ($\Delta\_acc < \Delta th$): {counter_down $+= 1$}; For 1 second, if (counter_down $\geq$ ODR/3) { $\Delta th -= 0.2$}

- Counter_down: When weaker vibrations cause less variation on acceleration, so the threshold decreases.

An update resolution is an input for the model. The Δth changes by adding or subtracting this value. More significant-resolution faster updates but it can exceed the proper value. In contrast, a smaller resolution will update slower but more precise. This working concept is based on gradient descent principle [32]. According to the theory of Nyquist frequency, the input frequency should be less than half of the sampling rate of the concerned signal. If Δ_{acc} of multiple vibrations continuously differ from Δth, it means that this Δth must be adjusted to follow the current situation of vibration. The Δth is updated when vibrations cause Δ_{acc} different to Δth with frequency more than Output Data Rate (ODR)/3 for a second. The updated model is described as Tab. 1, with an update resolution is 0.2 mg.

At this point, the threshold is updated in real-time and enhances the precision of the OACP for inclination measurement.

C. FUSION FILTER

Like the Kalman_acc filter, the Fusion filter combines 2 filters: OACP filter and LP filter. The inclination measurement from the acceleration of the LP filter contains the fast-dynamic response, which is fused with the high vibration immunity data from the OACP filter as an improved version of the OACP algorithm in Fig.16

$$Roll\_fusion = \beta \times Roll\_OACP + (1-\beta) \times Roll\_LP \quad (11)$$
$$Pitch\_fusion = \beta \times Pitch\_OACP + (1-\beta) \times Pitch\_LP \quad (12)$$

IV. EXPERIMENTAL SETUP

The involved sensors in experimental data are the LSM9DS1 from STMicroelectronics. This device is a system-in-package featuring a tri-axial digital linear acceleration sensor, gyroscope and magnetometer [33]. In the experiment, the accelerometer scale is $\pm$ 2g and the gyroscope range is 245 degrees per second. The magnetometer is not included in this project.

The implementation of the algorithms was made on an ARM Cortex-M4 based microcontroller STM32F401RE by STMicroelectronics [34], [35]. The MCU is assembled on its development board ST NUCLEO-F401RE [36], [37] for

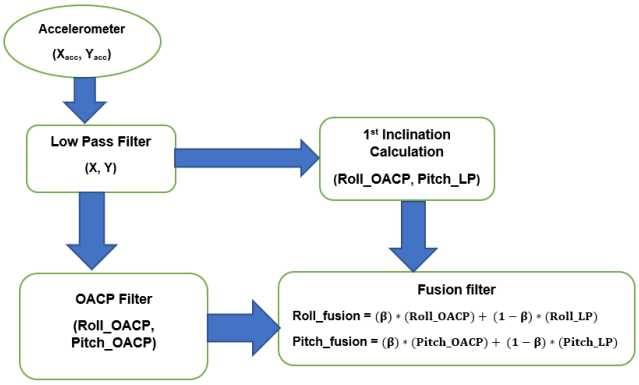

FIGURE 7. Fusion filter diagram.

easy accessibility to all the required connections. The sensor is mounted on the STEVAL-MKI159V1 adapter board [38] then it is connected to the MCU development via an Inter-Integrated Circuit (I2C) communication line.

A Pan-Tilt Uni Controller (PTU-C46) [39] with resolution 0.51° per position, provides fast and accurate positioning of cameras that is manipulated to verify the algorithm performance. The LSM9DS1 is assembled on PTU-C for tracking this device orientation. A TUMAC's Vibrator [40] is used to generate the vibration with a frequency of 50 Hz (3000 cycles per minute). All the acquisition data are sent to the host computer for signal analysis via USB cable from the nucleo-board.

The experiment contains the list of components, as demonstrated in Fig. 8

1) NUCLEO-F401RE Board
2) LSM9DS1 Sensor mounted on a Printed Circuit Board
3) Vibrator
4) AC/DC Power Supply
5) RS232 cable
6) PTU-C Controller
7) PTU-C46 Pan Tilt Unit
8) Heavy clamps

V. EXPERIMENTAL ANALYSIS

To achieve a stable transferring signal between the sensor and the computer, the ODR of accelerometer and gyroscope were set to 119 Hz. The gyroscope data were only used in the traditional Kalman filter.

After multiple tests, the best value of adjustable parameters for each algorithm were chosen to obtain the optimized performances as follows:

- LP coefficient: $\alpha = 0.9$
- Kalman uncertainties: $Q = 0.1, R = 0.0006$
- Fusion Filter coefficient: $\beta = 0.2$
- Starting threshold: ΔX threshold = ΔY threshold = $1mg$

The LP filter coefficient was chosen to remove the noise effectively but still guarantees the dynamic response, also with the concern of Nyquist theory.

The Kalman uncertainties were considered, based on the sensor datasheet.

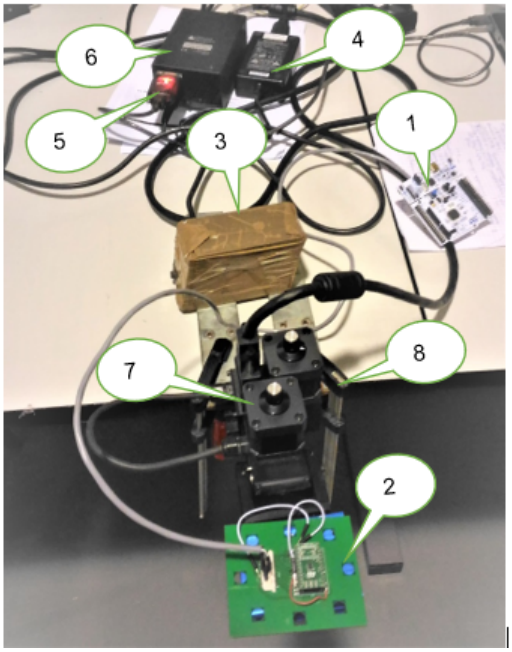

FIGURE 8. Fusion filter diagram.

TABLE 2. Reported data: before and after LP filter.

Abs Variation parameters	No filter	LP filter
Pitch mean (°)	5.184	0.654
Pitch max (°)	13.424	1.701
Pitch Std (°)	3.518	0.391
Roll mean (°)	3.863	0.346
Roll max (°)	10.152	0.999
Roll Std (°)	2.183	0.238

The Fusion Filter coefficient should be in a compromise between the OACP filter and LP filter. Higher β leads the signal more like the OACP output (better in noise removal). Smaller β provides more characteristics of LP filter for the signal (faster dynamic response). With $\beta = 0.2$, the signal removes the noise effectively with a better dynamic response.

The starting threshold is significant enough based on the OACP working principle. Moreover, this value can be updated automatically during operation.

A. LP FILTER VERIFICATION

To guarantee the efficiency of the LP filter, a quick experiment is carried out. The sensor is horizontally placed on the vibrator for 1 minute, and then the result is reported in Tab. 2 to verify the performance of the LP filter. As shown in Fig 9 the LP filter significantly reduces noise from raw measurement that confirms the success of LP filter design in noise removal.

- No filter vs LP filter

The maximum spike decreases from more than 10° to less than 1.8° for both roll and pitch. Mean and standard deviation (std) values are minimized noticeably.

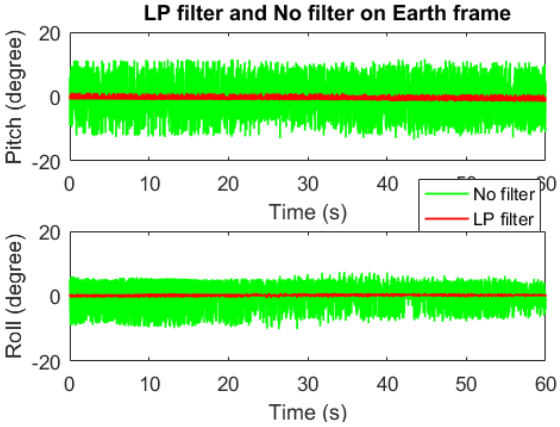

FIGURE 9. Noise deduction by LP filter.

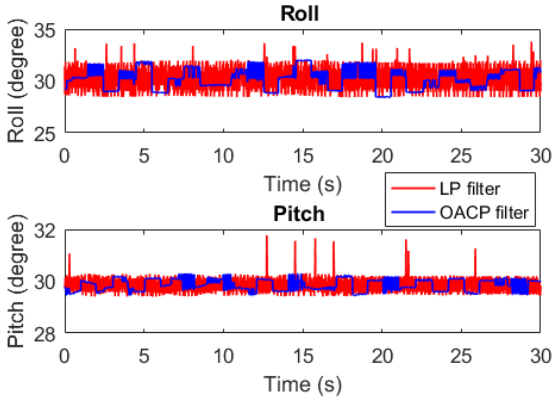

FIGURE 10. LP and OACP on slope of 30°.

B. INCLINATION TEST

A robust setup was set up as shown in Fig. 8. Different from the previous test, the sensor is mounted on the PTU-C controller, so the vibration is more robust due to the interaction between the vibrator and mechanical parts of the device. All the algorithms are processed based on this system to see the difference in each filter To analyze the behavior of the OACP filter on inclination, roll, and pitch were controlled to tilt alternately at 15°, 30°, and 45° for 30 s. This test characterized how the LP filter change after OACP optimization on inclination. Fig. 10 shows the signal of the LP filter before and after the OACP process on a slope of 30°. The LP performance is improved thanks to the optimization of the OACP technique significantly. The spikes are restrained clearly, and the acquired signal becomes more stable with less variation.

As reported in Tab. 3, vibration conducts in roll more seriously than pitch so roll data suffers considerable variation. On the other hand, the OACP adapts well with various inclinations where the spikes as well as vibrated behavior, always minor apparently. Besides, the mean value of oriental position is maintained closer to the reference by the OACP technique.

C. FILTER COMPARISON

- For the static test, the sensor is kept on the Earth frame, which does not incline for 60 seconds to observe how the vibration impact on each filter.

TABLE 3. Vibration impact on the inclinations.

Parameter	Oriental Reference					
	LP filter			After OACP filter		
	15°	30°	45°	15°	30°	45°
Roll mean	15.42	30.29	45.85	15.40	30.24	45.44
Roll most	3.12	3.79	2.03	1.35	1.80	0.89
Roll std	0.69	1.07	0.54	0.59	0.80	0.33
Pitch mean	15.06	29.85	44.42	15.03	29.94	44.55
Pitch most	1.53	1.77	2.15	0.44	0.30	0.23
Pitch std	0.19	0.27	0.33	0.17	0.22	0.32

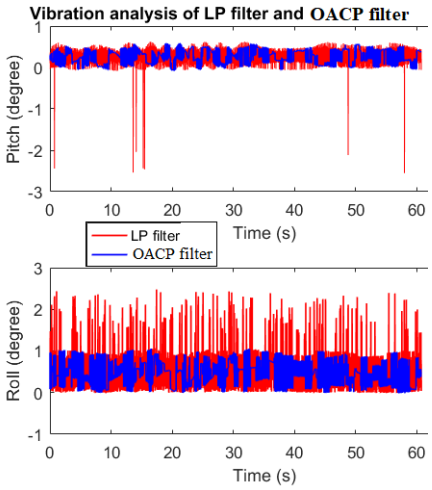

FIGURE 11. LP filter and OACP filter on earth frame.

- For the dynamic test, the pitch is rotated from 10° to 60° then the roll is rotated from −10° to 30° about ten cycles for each test. There are short periods of static position between peak to peak and cycle to cycle. A large quantity of data is acquired. The characteristics of the filter behavior are inspected via the way each algorithm reacts to vibration and also time response to dynamic motion

1) STATIC TEST

- LP filter vs. OACP filter

Like the previous test, the OACP filter is applied to the LP filter to observe the optimization of the proposed method. As shown in Fig.11, the OACP filter restrains the strange spikes of inclination measurement. This improvement is advantageous to keep the right result from sudden change caused by vibration.

- OACP vs. Fusion filter characteristic

In this part, the processing behaviors of the OACP filter and Fusion filter are analyzed to observe the pros and cons of each type of filter. The acquisition value of the Fusion filter varies back and forth more closely to 0 than the OACP filter, as shown in Fig.12 and Fig.13. The OACP filter is less vulnerable to the vibratory influence. However, once

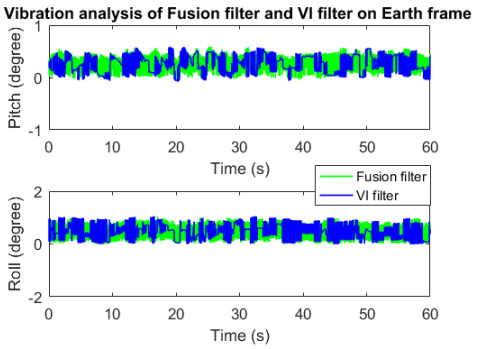

FIGURE 12. Fusion filter and OACP filter on earth frame.

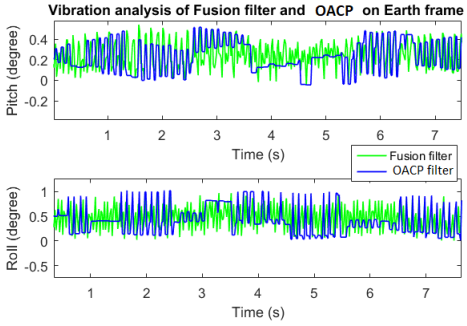

FIGURE 13. Behavior of fusion filter and OACP filter.

TABLE 4. The vibration impact on filters (degree).

Abs Variation parameter	LP Filter	OACP filter	Fusion filter	Kalman filter	Kalman _acc
Pitch mean (°)	0.26	0.25	0.25	0.25	0.25
Pitch max (°)	2.55	0.58	0.59	0.61	0.62
Pitch Std (°)	0.19	0.17	0.14	0.16	0.16
Roll mean (°)	0.55	0.4	0.46	0.47	0.46
Roll max (°)	2.47	1.05	1.05	1.06	1.05
Roll Std (°)	0.43	0.27	0.26	0.3	0.3

it is affected, the signal remains at the fluctuated value for longer than what happened with the fusion filter. Therefore, the mean value of the OACP filter is higher than the Fusion filter, as reported in Tab. 4.

- Filter fusion vs. Kalman filter vs. Kalman_acc filter

The Fusion filter behaves quite similarly to the Kalman filter. Meanwhile, the Kalman filter and Kalman_acc filter are nearly the same with a minimal variation, like Fig.14 and Fig.15.

Tab. 4 reports data of all algorithms during vibration impact for 60 s. The LP filter has an enormous variation caused by vibration. The OACP filter and Fusion filter achieve the best performance in the term of vibration immunity. Meanwhile, 2 Kalman filters are competitive with each other, with a slight difference only.

2) DYNAMIC TEST

In the dynamic experiment, the dynamic behavior and time response of each filter is evaluated appropriately. Each time,

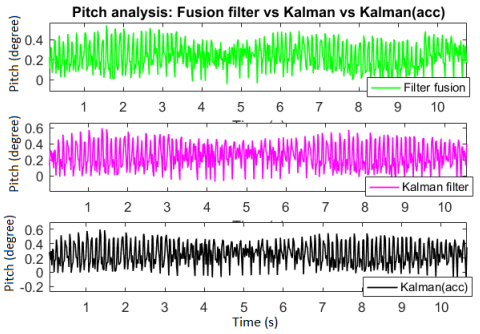

FIGURE 14. Pitch of filter fusion vs. Kalman filter vs. Kalman_acc filter on earth frame.

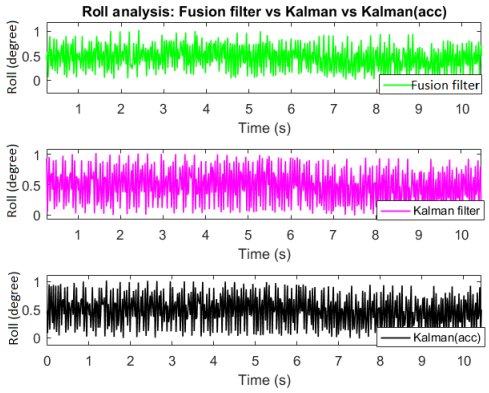

FIGURE 15. Roll of filter fusion vs. Kalman filter vs. Kalman_acc filter on earth frame.

the PTU-C finishes its motion, it rests at a static position for a short time to observe the inclination.

- Pitch dynamic rotation

Here, the LP filter is red line, OACP filter is blue line, and Fusion filter is green line.

LP, OACP, and Fusion filter - as seen in the dynamic behavior of pitch in Fig.16 and Fig.17, the OACP filter reaches the static value by step movement. Unlike LP and Fusion filter, the OACP filter has the trend to calculate the value directly when the sensor ends its rotation. Although the OACP filter has more stable at static situation, sometimes it gets a small delay compared with the LP filter. This feature is improved in the Fusion filter with better dynamic behavior with the combination of the noise removal of the OACP filter and the fast-dynamic response of the LP filter.

- Roll dynamic rotation

The roll is controlled to rotate from $-10°$ to $30°$. As mentioned above, the OACP filter can generate delays occasionally. However, it is more stable for the static parameter, as shown in Fig.18. The Fusion filter does not have strange spikes like the LP filter and accomplishes the last value nearly at the same time with the LP filter.

LP filter and 2 Kalman filters - as shown in Fig.19 and Fig.20, the behavior of the Kalman filter and Kalman_acc filter are close to each other. They have a good dynamic response and make the signal smoother, with respect to the

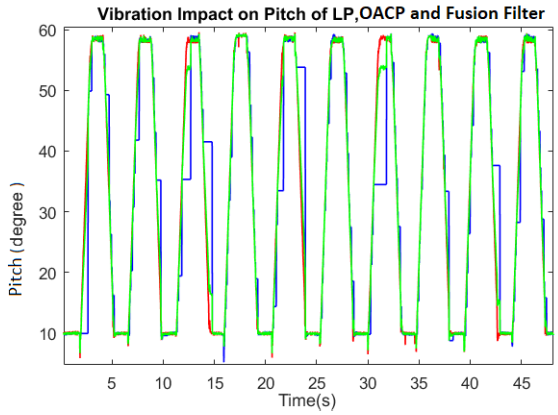

FIGURE 16. LP, OACP, fusion filter dynamic motion.

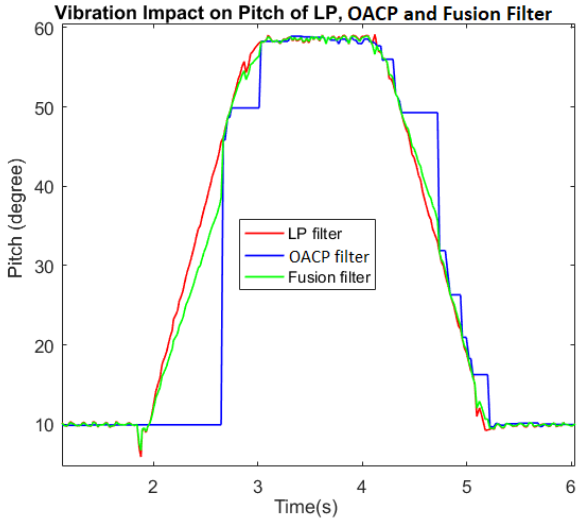

FIGURE 17. Pitch of LP, OACP and fusion filter behavior.

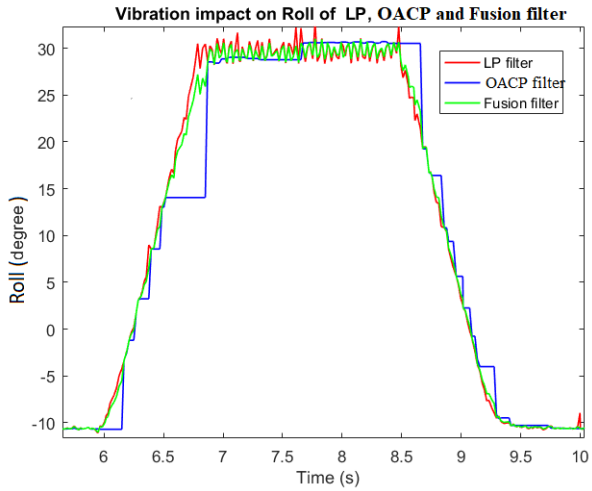

FIGURE 18. Roll of LP, OACC and fusion filter behavior.

LP filter. Related to the static parameters, the Kalman filters remove the noise effectively for both dynamic cases of roll and pitch. Despite the corresponding performance,

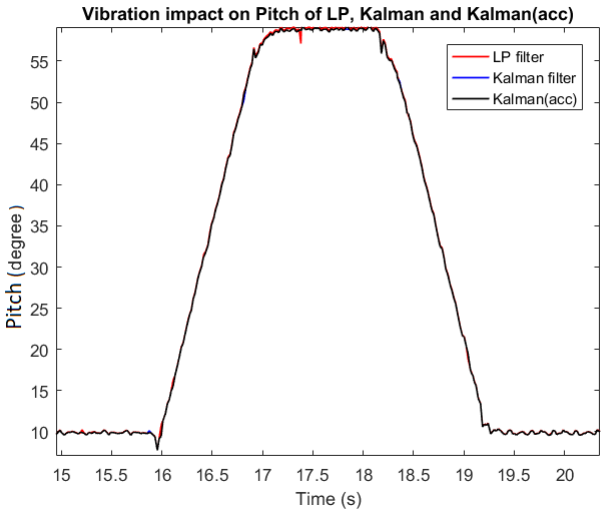

FIGURE 19. Pitch of LP and 2 Kalman filters behavior.

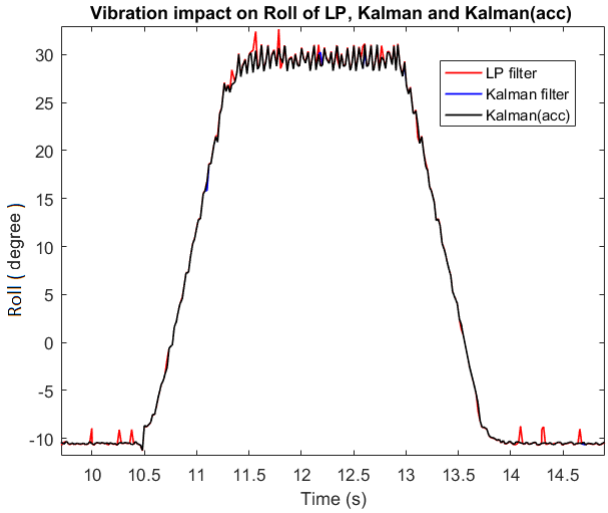

FIGURE 20. Roll of LP and 2 Kalman filters behavior.

a significant advantage of Kalman_acc filter is the processing operation with the absence of gyroscope.

- Pitch dynamic rotation
- Roll dynamic rotation

3) DYNAMIC TIME RESPONSE

Practically, the user wants to receive the inclination measurement as fast as possible when the sensor is stopped its motion. Therefore, two important parameters should be considered:

- Time_rise: from the starting time of motion from low to high until staying at a maximum stable value.
- Time_down: from the starting time of motion from high to low until staying at a minimum stable value.

The rotating speed of PTU-C is 50°/second. To make the comparison in terms of dynamic time, the mean time value of 10 cycles is calculated from the above dynamic motion: pitch (10° to 60°), roll (−10° to 30°), as shown in Tab. 5 and Tab. 6. All the units are reported in second, and the dynamic

TABLE 5. Dynamic mean time of pitch (10 cycles).

Dynamic time	LP filter	OACP filter	Fusion filter	Kalman filter	Kalman_acc filter
Time_rise (s)	1.03	1.171	1.171	1.036	1.03
Time_down (s)	1.157	1.425	1.223	1.163	1.163

TABLE 6. Dynamic mean time of roll (10 cycles).

Dynamic time	LP filter	OACP filter	Fusion filter	Kalman filter	Kamanl_acc filter
Time_rise (s)	0.808	0.853	0.812	0.808	0.808
Time_down (s)	0.827	0.888	0.848	0.827	0.827

motion always suffers the vibration impact. The reference time of the dynamic pitch, dynamic roll are 1 second and 0.8 second respectively for each Time_rise or Time_down.

Generally, all the filters performed a good dynamic response, compared with time reference. The small delay values can be understood by the vibration impact and serial transmission time. During the dynamic rotation, Time_rise is faster than Time_down.

The reported data from Tab. 5 and Tab. 6 indicate that the dynamic time of the LP filter and 2 Kalman filters are close to each other. The sensor fusion Kalman is slower than Kalman_acc filter only in Time_rise of the pitch.

The dynamic time of the OACP filter is improved in the Fusion filter but still requires a longer time to attain the stable value, respected to Kalman filters.

VI. CONCLUSION

This work has introduced a new algorithm with the practical principle to optimize the vibration impact based on the MEMS accelerometer with the absence of other sensors. The inclinational measurements were analyzed in detail for static and dynamic cases. The OACP filter can work independently and remove the considerable spikes from the LP filter. Furthermore, its dynamic performance in terms of time is apparently improved by fusing with the LP filter and Kalman algorithm. The Kalman_acc filter shows a highly competitive accomplishment with the traditional Kalman filter, which requires gyroscope support. This research relief the burden on the LP filter and also solves the economic problem in the industrial inclinometer in dealing with the external noise without sensor fusion.

REFERENCES

[1] A. Harindranath and M. Arora, "MEMS IMU sensor orientation algorithms-comparison in a simulation environment," in *Proc. Int. Conf. Netw., Embedded Wireless Syst. (ICNEWS)*, Dec. 2018, pp. 1–6.

[2] G. Qinglei, L. Huawei, M. Shifu, and H. Jian, "Design of a plane inclinometer based on MEMS accelerometer," in *Proc. Int. Conf. Inf. Acquisition*, Jul. 2007, pp. 320–323.

[3] S. Hosseinyalamdary, Y. Balazadegan, and C. Toth, "Tracking 3D moving objects based on GPS/IMU navigation solution, laser scanner point cloud and GIS data," *ISPRS Int. J. Geo-Inf.*, vol. 4, no. 3, pp. 1301–1316, Jul. 2015.

[4] G. Nützi, S. Weiss, D. Scaramuzza, and R. Siegwart, "Fusion of IMU and vision for absolute scale estimation in monocular SLAM," *Unmanned Aerial Vehicles*, vol. 61, no. 1, pp. 287–299, 2010.

[5] G. Lan, Y. Bu, J. Liang, and Q. Hao, "Action synchronization between human and UAV robotic arms for remote operation," in *Proc. IEEE Int. Conf. Mechatronics Automat.*, Aug. 2016, pp. 2477–2481.

[6] S.-O. Shin, D. Kim, and Y.-H. Seo, "Controlling mobile robot using IMU and EMG sensor-based gesture recognition," in *Proc. 9th Int. Conf. Broadband Wireless Comput., Commun. Appl.*, Nov. 2014, pp. 554–557.

[7] P. Schopp, H. Graf, W. Burgard, and Y. Manoli, "Self-calibration of accelerometer arrays," *IEEE Trans. Instrum. Meas.*, vol. 65, no. 8, pp. 1913–1925, Aug. 2016.

[8] J. Wang, G. Gao, and P. Liu, "The study on lange-angle CANBUS 2-axis inclinometer of rotary drilling rig," in *Proc. 2nd IEEE Int. Conf. Inf. Manage. Eng.*, 2010, pp. 95–97.

[9] Z. Chen, H. Li, X. Du, and J. Yan, "Research on the calibration method of MEMS accelerometer based on recursive least squares," in *Proc. IEEE Int. Conf. Mechatronics Automat. (ICMA)*, Aug. 2018, pp. 533–538.

[10] L. Da-Wei and G. Tao, "Design of dual-axis inclinometer based on MEMS accelerometer," in *Proc. 3rd Int. Conf. Measuring Technol. Mechatronics Automat.*, Jan. 2011, pp. 959–961.

[11] X. Lu and Z. Liu, "IEKF-based self-calibration algorithm for triaxial accelerometer," in *Proc. 3rd Int. Conf. Inf. Sci. Control Eng. (ICISCE)*, Jul. 2016, pp. 983–987.

[12] B. Suwandi, T. Kitasuka, and M. Aritsugi, "Vehicle vibration error compensation on IMU-accelerometer sensor using adaptive filter and low-pass filter approaches," *J. Inf. Process.*, vol. 27, pp. 33–40, Jan. 2019, doi: 10.2197/ipsjjip.27.33.

[13] M. L. Hoang, A. Pietrosanto, S. D. Iacono, and V. Paciello, "Preprocessing technique for compass-less madgwick in heading estimation for industry 4.0," in *Proc. IEEE Int. Instrum. Meas. Technol. Conf. (IMTC)*, May 2020, pp. 1–6.

[14] M. L. Hoang, M. Carratù, V. Paciello, and A. Pietrosanto, "A new orientation method for inclinometer based on mems accelerometer used in industry 4.0," in *Proc. IEEE 18th Int. Conf. Ind. Inform. (INDIN)*, Jul. 2020.

[15] Y. A. Nekrasov, S. V. Pavlova, and N. V. Moiseev, "MEMS gyro vibration immunity and its measurement with TIRA shaker," in *Proc. IEEE Int. Instrum. Meas. Technol. Conf. (IMTC)*, May 2015, pp. 1763–1768.

[16] J. Chang, J. Cieslak, A. Zolghadri, J. Davila, and J. Zhou, "Design of sliding mode observers for quadrotor pitch/roll angle estimation via IMU measurements," in *Proc. Workshop Res., Educ. Develop. Unmanned Aerial Syst. (RED-UAS)*, Nov. 2015, pp. 393–400.

[17] Y. Zhong, Y. Xu, N. He, and X. Yu, "A new drone accelerometer calibration method," in *Proc. 37th Chin. Control Conf. (CCC)*, Jul. 2018, pp. 9928–9933.

[18] Y. Zhong and Y. Xu, "A calibration method of UAV accelerometer based on Levenberg-Marquardt iteration algorithm," in *Proc. Chin. Control Decis. Conf. (CCDC)*, Jun. 2018, pp. 5634–5638.

[19] S. Sabatelli, M. Galgani, L. Fanucci, and A. Rocchi, "A double-stage Kalman filter for orientation tracking with an integrated processor in 9-D IMU," *IEEE Trans. Instrum. Meas.*, vol. 62, no. 3, pp. 590–598, Mar. 2013.

[20] Y. Zhao, "Cubature + extended hybrid Kalman filtering method and its application in PPP/IMU tightly coupled navigation systems," *IEEE Sensors J.*, vol. 15, no. 12, pp. 6973–6985, Dec. 2015.

[21] B. Karahoda, X. Mehmeti, and U. Cabra, "Noise reduction in quadcopter accelerometer and gyroscope measurements based on Kalman filter," in *Proc. UBT Int. Conf.*, Nov. 2015, pp. 1–6.

[22] B. Huyghe, J. Doutreloigne, and J. Vanfleteren, "3D orientation tracking based on unscented Kalman filtering of accelerometer and magnetometer data," in *Proc. IEEE Sensors Appl. Symp.*, Feb. 2009, pp. 148–152.

[23] X. Wang, J. Guo, and N. Cui, "Adaptive extended Kalman filtering applied to low-cost MEMS IMU/GPS integration for UAV," in *Proc. Int. Conf. Mechatronics Automat.*, Aug. 2009, pp. 2214–2218.

[24] W. Wang and P. G. Adamczyk, "Comparison of bingham filter and extended Kalman filter in IMU attitude estimation," *IEEE Sensors J.*, vol. 19, no. 19, pp. 8845–8854, Oct. 2019.

[25] L. D. Paarmann, *Design and Analysis of Analog Filters: A Signal Processing Perspective*. Norwell, MA, USA: Kluwer, 2001.

[26] J. Chen, X. Ni, and B. Mo, "A low noise CMOS charge sensitive preamplifier for MEMS capacitive accelerometer readout," in *Proc. 7th Int. Conf. ASIC*, Oct. 2007, pp. 490–493.

[27] A. Sofwan, Sumardi, and N. Ulwiyati, "Filtering for data acquisition on wireless sensor network," in *Proc. 5th Int. Conf. Inf. Technol., Comput., Electr. Eng. (ICITACEE)*, Sep. 2018, pp. 180–184.
[28] M. Carratu, S. D. Iacono, M. L. Hoang, and A. Pietrosanto, "Energy characterization of attitude algorithms," in *Proc. IEEE 17th Int. Conf. Ind. Informat. (INDIN)*, Jul. 2019, pp. 1585–1590.
[29] P. Promrit, S. Chokchaitam, and M. Ikura, "In-vehicle MEMS IMU calibration using accelerometer," in *Proc. IEEE 5th Int. Conf. Smart Instrum., Meas. Appl. (ICSIMA)*, Nov. 2018, pp. 1–3.
[30] L. Cocco and S. Rapuano, "Accurate speed measurement methodologies for formula one cars," in *Proc. IEEE Instrum. Meas. Technol. Conf. (IMTC)*, May 2007, pp. 1–6.
[31] H. Ferdinando, H. Khoswanto, and D. Purwanto, "Embedded Kalman filter for inertial measurement unit (IMU) on the ATMega8535," in *Proc. Int. Symp. Innov. Intell. Syst. Appl.*, Jul. 2012, pp. 1–5.
[32] H. Jaber and M. Frye, "Laguerre polynomials and gradient descent approach for linear quadratic optimal control," in *Proc. 7th Int. Conf. Electr. Electron. Eng. (ICEEE)*, Apr. 2020, pp. 281–284.
[33] *iNEMO Inertial Module: 3D Accelerometer, 3D Gyroscope, 3D Magnetometer—Data Sheet*, STMicroelectronics, Geneva, Switzerland, Mar. 2015.
[34] *Ultra-Low-Power ARM Cortex-M4 32-Bit MCU+FPU, 105 DMIPS, 512KB Flash/96KB RAM, 11 TIMs, 1 ADC, 11 comm. Interfaces*, STMicroelectronics, Geneva, Switzerland, Jan. 2015.
[35] *STM32F401XB/C and STM32F401XD/E Advanced ARM-Based 32-Bit MCUs*, STMicroelectronics, Geneva, Switzerland, Dec. 2018.
[36] *STM32 Nucleo-64 Boards—Product Specifications*, STMicroelectronics, Geneva, Switzerland, Oct. 2018.
[37] *STM32 Nucleo-64 Boards—User Manual*, STMicroelectronics, Geneva, Switzerland, Dec. 2017.
[38] *LSM9DS1 Adapter Board for a Standard DIL24 Socket*, STMicroelectronics, Geneva, Switzerland, Sep. 2016.
[39] *Pan-Tilt Unit (Model PTU) User's Manual*, Rollins Road Burlingame, Directed Perception, Inc., Burlingame, CA, USA, Oct. 2000.
[40] *Vibratory Feeders—San Giuliano Milanese—Milan*, Tumac, Vancouver, WA, USA, 2015.

MINH LONG HOANG (Member, IEEE) was born in Hanoi, Vietnam, in 1994. He received the B.S. degree in renewable energy from the University of Science and Technology of Hanoi, Vietnam, in 2015, and the M.S. degree in electronic engineering from the University of Salerno, Italy, in 2018, where he is currently pursuing the Ph.D. degree, working on the Nationally Operative Program (PON) Project of European Union about "Industry 4.0 Oriented Enhancement of Inertial Platform Performance." Also within this project, he has been collaborating with Sensor System Srl Company, Italy, and Baumer Company, Germany, as a Researcher with the Research and Development Department in the field of inclinometer. His research interests include inertial measurement unit (IMU) sensors, microelectromechanical systems (MEMSs), real-time measurements, embedded systems, and signal processing.

ANTONIO PIETROSANTO (Senior Member, IEEE) was born in Naples, Italy, in 1961. He has been a Full Professor of electrical and electronic measurement with the University of Salerno, since 2001. He has been the Founder of three spin off of the University of Salerno: "SPRING OFF," "Metering Research," and "Hippocratica Imaging." He has coauthored more than 150 papers in international journals and conference proceedings. His main research interests include instrument fault detection and isolation (IFDIA), sensors, WSNs, real-time measurements, embedded systems, metrological characterization of measurement software, advanced system for food quality inspection, and image-based measurements.